PHASE RESETTING AND BIFURCATION IN THE VENTRICULAR MYOCARDIUM

TERESA REE CHAY* AND YOUNG SEEK LEE‡
*Departments of *Biological Sciences and ‡Chemistry, University of Pittsburgh, Pittsburgh, Pennsylvania 15260*

ABSTRACT With the dynamic differential equations of Beeler, G. W., and H. Reuter (1977, *J. Physiol.* [*Lond.*]. 268:177–210), we have studied the oscillatory behavior of the ventricular muscle fiber stimulated by a depolarizing applied current I_{app}. The dynamic solutions of BR equations revealed that as I_{app} increases, a periodic repetitive spiking mode appears above the subthreshold I_{app}, which transforms to a periodic spiking-bursting mode of oscillations, and finally to chaos near the suprathreshold I_{app} (i.e., near the termination of the periodic state). Phase resetting and annihilation of repetitive firing in the ventricular myocardium were demonstrated by a brief current pulse of the proper magnitude applied at the proper phase. These phenomena were further examined by a bifurcation analysis. A bifurcation diagram constructed as a function of I_{app} revealed the existence of a stable periodic solution for a certain range of current values. Two Hopf bifurcation points exist in the solution, one just above the lower periodic limit point and the other substantially below the upper periodic limit point. Between each periodic limit point and the Hopf bifurcation, the cell exhibited the coexistence of two different stable modes of operation; the oscillatory repetitive firing state and the time-independent steady state. As in the Hodgkin-Huxley case, there was a low amplitude unstable periodic state, which separates the domain of the stable periodic state from the stable steady state. Thus, in support of the dynamic perturbation methods, the bifurcation diagram of the BR equation predicts the region where instantaneous perturbations, such as brief current pulses, can send the stable repetitive rhythmic state into the stable steady state.

INTRODUCTION

The rhythm of autonomous biological oscillators, such as neural and cardiac oscillators, can be reset or annihilated by brief perturbations (1). Best (2) has investigated phase resetting behavior in the Hodgkin-Huxley equations (3), which represent quantitative expressions for the ionic events in the squid axon membrane. He found that voltage perturbations to the axon given at points along its firing spike result in advance, delay, or even permanent cessation of periodic firing, depending on the strength of perturbations. Guttman et al. (4) have shown that repetitive firing in space-clamp squid axons bathed in low calcium and stimulated by a depolarizing applied current can be annihilated by a brief depolarizing or hyperpolarizing current pulse of the proper magnitude applied at the proper phase. Rinzel (5) and Rinzel and Miller (6) have calculated period solutions to the space-clamped Hodgkin-Huxley equations as a function of depolarizing applied current. They found that in a region where a stable periodic solution coexists with a stable steady solution, there is an additional periodic solution that is unstable. In addition, they found that at 6.3 °C the limb of unstable solutions has a switch-back region so that for some applied current values this limb exhibits three unstable limit cycles.

In sinus node cells of cat (7) and in the isolated Purkinje fiber of dog (8), Jalife and Antzelevitch found that spontaneous firing can be terminated by giving a brief current stimulus at the right moment. The model of McAllister et al. (10), which quantitatively describes the rhythmic activity of Purkinje fiber, also predicts the phase resetting phenomenon and annihilation of the rhythmic activity, in the presence of a constant depolarizing current (9).

The propagation of an impulse through the heart depends upon excitability properties associated with the cell membranes and the pattern of interconnection between the cells. Our mathematical analysis of the phase resetting behavior of the ventricular muscle cells was motivated by a desire to obtain insight into the dynamics of oscillations in response to a brief current pulse on the cell linked electrically to the Purkinje fiber. We also wanted to see whether this cell exhibits the phase resetting behavior similar to that found with the Purkinje fiber (9).

Although the ventricular muscle cell is electrically silent and does not produce rhythmic activity, it has been demonstrated experimentally (11) that a steady depolarizing applied current brings about oscillatory potentials from a resting ventricular muscle fiber. The quantitative model of Beeler and Reuter (12) (BR) not only accounts for this experimental observation, but also recreates many of the electrical phenomenon associated with ionic concentration changes and drug effects.

Here we have performed a bifurcation analysis on the

membrane potential of the ventricular myocardium using a bias applied current as a bifurcation parameter. In addition, we have carried out numerical simulations on the dynamics of action potentials in response to brief impulses to study its phase resetting behavior. Since the BR-model includes expressions for the ion channels in the cell membrane, by changing appropriate parameters, our simulations suggest additional experiments that might elucidate the role of channel blocking drugs on phase resetting behavior. Investigating the interactions between the model parameters and the phase resetting phenomenon for a single pacemaker is the first step toward understanding the cause of cardiac arrhythmias, the clinical relevance of which is apparent.

METHOD AND RESULTS

For our study, we have used the quantitative description of electrical activity of the ventricular muscle fiber formulated by Beeler and Reuter (12). The set of equations and the parametric values were taken from Table I of reference 12. Their model consists of a system of eight first-order, simultaneous, nonlinear differential equations that include: An initial fast inward current carried primarily by sodium ions, I_{Na}, that is responsible for the fast depolarizing phase; a secondary or slow inward current, I_s, carried mainly by calcium ions whose resting potential varies with the intracellular calcium concentration; a time-independent potassium outward rectification current I_{K1}, that increases on depolarization; finally, a time-dependent slow outward current I_{x1} carried by K^+ ions.

In Fig. 1, we examined the action potential of the myocardium by means of bifurcation analysis. We used the AUTO, a program for the automatic bifurcation analysis developed by Doedel (15), to construct this diagram. This analyzer computes the regions of the periodic branches,

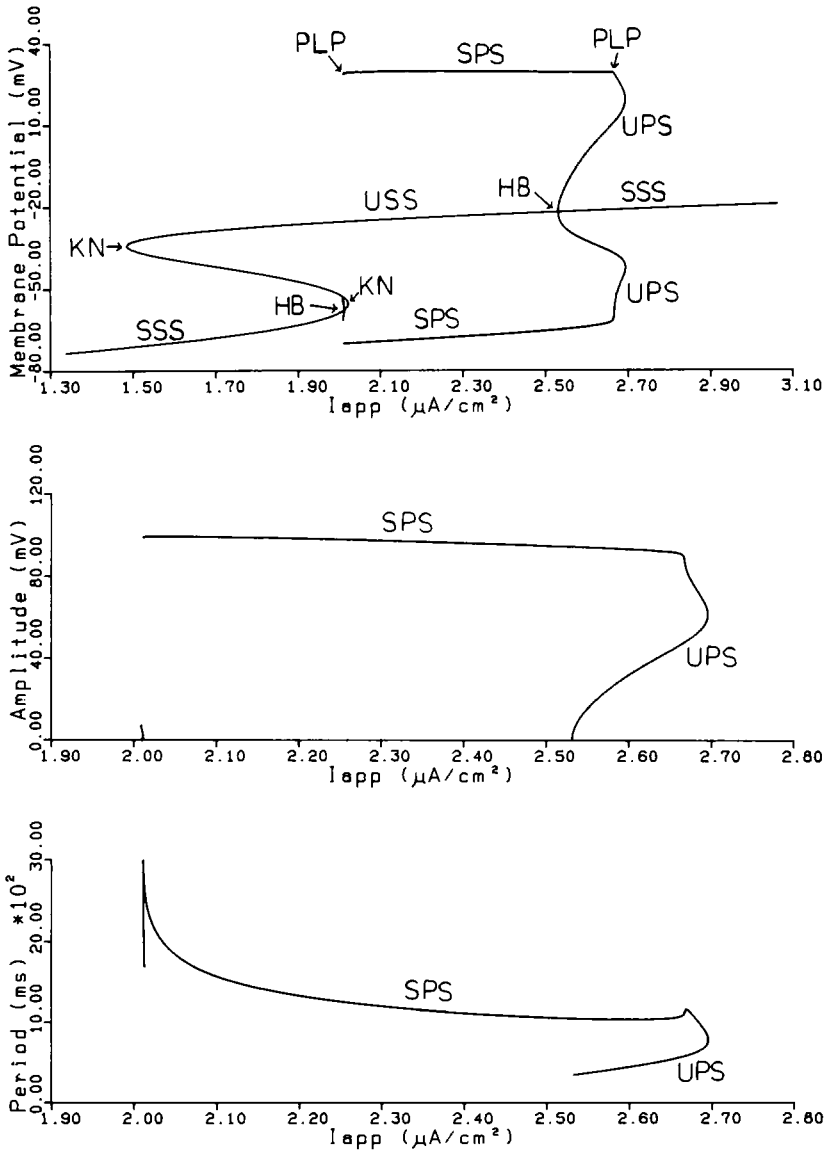

FIGURE 1 Bifurcation diagram of the BR equations that reveals autonomous rhythm of the myocardial cell as a function of I_{app}, an external depolarizing current. From the *top* trace to the *bottom*, we show the membrane potential, amplitude, and period as a function of I_{app}, respectively. Here, *HB* stands for the Hopf bifurcation point, *KN* for the knee, *SSS* for the stable steady state, *USS* for the unstable steady state, *SPS* for the stable periodic state, *UPS* for the unstable periodic state, and *PLP* for the periodic limit point.

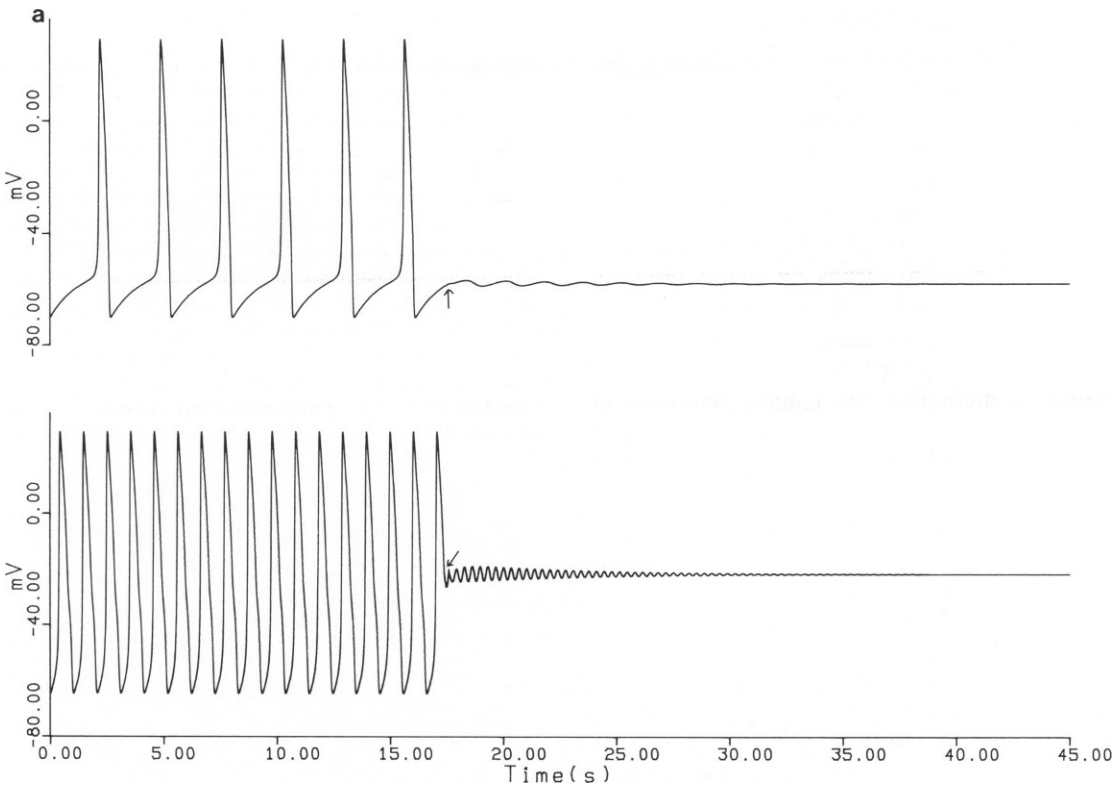

FIGURE 2 (*a*) Dynamic behavior of the ventricular muscle fiber brought about by applying a steady applied current strength of $+2.01$ $\mu A/cm^2$ (*top*, near left *HB*) and $+2.56$ $\mu A/cm^2$ (*bottom*, near right *HB*). In the *top* trace, a brief current of -0.005 $\mu A/cm^2$ and of duration of 200 ms is applied at -57.7 mV of the upstroke (i.e., at the arrow shown); in the *bottom* trace, a brief current of -0.25 $\mu A/cm^2$ and of the same duration given at -2.16 mV of the downstroke results in a permanent cessation of the rhythm. (*b*) Oscillations of three ionic currents near the current pulse in *a* are shown. Here, the *top* and *bottom* traces correspond to those of *a*, respectively.

steady state branches, and Hopf bifurcation points. It also gives the amplitude and period at a given value of the bifurcation parameter. The top of Fig. 1 shows the membrane potential as a function of I_{app}, an externally applied current. The middle and bottom rows show the amplitude and period, respectively. Note that there are two Hopf bifurcation points (HB); one at 2.013 $\mu A/cm^2$ (its membrane potential at -57.69 mV) and another one at 2.532 $\mu A/cm^2$ ($V_m = -21.78$ mV); two knees (KN) appear at 1.484 $\mu A/cm^2$ ($V_m = -34.07$ mV) and 2.022 $\mu A/cm^2$ (-55.46 mV); stable periodic states (SPS) exist between 2.011 and 2.672 $\mu A/cm^2$. The unstable periodic state (UPS) extends to 2.695 $\mu A/cm^2$, where it oscillates between 19.18 and -42.15 mV. Note that near the two HBs, the BR equations have a stable oscillatory state (SPS) coexistent with a stable steady state (SSS); these two states are separated by an unstable oscillatory state (UPS); i.e., the unstable periodic branch (UPS) connects the stable periodic limit point (PLP) and the Hopf bifurcation (HB).[1] In these regions, instantaneous perturbations such as a brief current pulse may send stable repetitive activity into the steady state; i.e., into one of the shaded areas in Fig. 8.

A bifurcation approach, however, is limited in that it does not give the dynamic results. The dynamic solutions can be obtained by solving the full dynamic equations, and we have done so numerically using the B-R differential equations on a DEC 10 (Digital Equipment Corp., Marlboro, MA) computer using a Gear algorithm (13). To increase an accuracy of the computation we used double precision with the absolute and relative error tolerances set at 10^{-8}. We have checked the accuracy of our results (i.e., the maximum and minimum of the membrane potential, amplitude, period) by comparing with those given in the bifurcation diagram of Fig. 1 and found close agreement between the two methods.

Fig. 2 *a* compares the oscillatory modes at two different regions of the bifurcation diagram and the approaches to their respective steady states when a brief current pulse of the proper magnitude is given at the appropriate phase of the oscillatory cycle. Here, the two systems were initially at the repetitive states: the system at $I_{app} = 2.01$ $\mu A/cm^2$ (the top trace) and that at $I_{app} = 2.56$ $\mu A/cm^2$ (the bottom trace). In the top trace, when a current pulse of -0.005 $\mu A/cm^2$ with 200-ms duration is given at -57.7 mV of the upstroke of a spike (i.e., at the arrow), the fiber quickly loses its rhythmic activity and approaches the steady state value of -57.8 mV. In the bottom trace, when the current strength of -0.25 $\mu A/cm^2$ with the same duration is given at -21.4 mV of the downstroke of a spike, the fiber slowly approaches the steady state value of -21.6 mV. Note that the system at a stronger applied current oscillates with a much higher frequency; this is also predicted from our bifurcation analysis (i.e., the period shown in the bottom trace of Fig. 1) and is in agreement with the Hodgkin-Huxley case (3, 4). Unlike the HH case (where the amplitude is smaller for higher I_{app}), however, the amplitude of the BR periodic branch remains almost constant for all values of I_{app} in the stable periodic region.

The top trace of Fig. 2 *b* reveals a perturbation in the Ca^{2+} current and time-dependent and time-independent K^+ currents, when a brief pulse of the equal magnitude and at the same phase in Fig. 2 *a* is given at the arrow. The bottom trace reveals a perturbation in those currents as a result of the pulse shown on the lower trace of Fig. 2 *a*. A perturbation in

[1]Professor Doedel has pointed out that the bifurcating branch of the periodic solution, which originates from the left Hopf bifurcation, terminates in a homoclinic orbit (i.e., orbit of infinite period containing a saddle point). Also, the left PLP terminates in another homoclinic orbit, forming a cusp with the former.

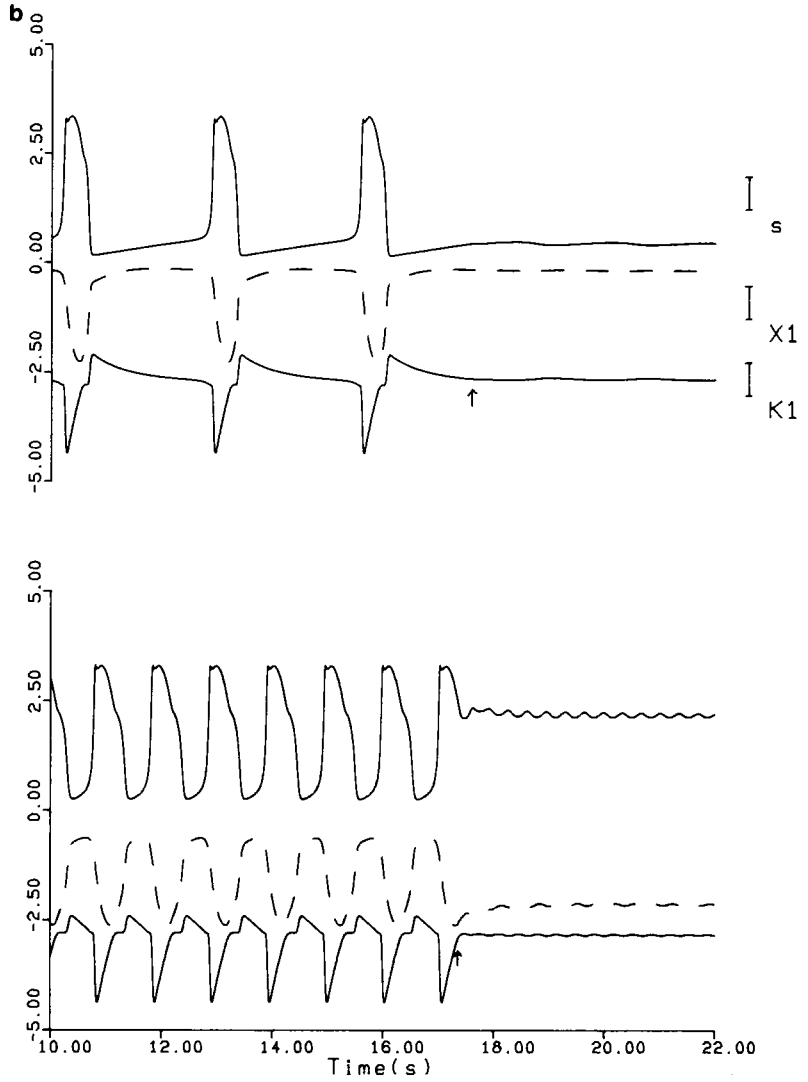

FIGURE 2 Continued

the Na^+ current is not displayed here because for I_{app} greater than the left Hopf bifurcation point the magnitude of the Na^+ current is almost negligible compared with the Ca^{2+} and K^+ currents and thus it does not contribute to annihilation of the rhythmic activity.

Near the right PLP, the action potential oscillates in a form of bursting-spiking modes as shown in Fig. 3. Here, the system originally at the applied current strength of 2.667 $\mu A/cm^2$ was instantaneously brought to a new state (i.e., close to the right PLP) by raising the strength to higher values (e.g., to 2.670 $\mu A/cm^2$ in the top trace and to 2.672 $\mu A/cm^2$ the bottom trace). Note from the bottom trace that the mode is chaotic in that the number of spikes varies from one burst to another. Perhaps it is worthwhile to point out that the bursting rhythm shown in this figure can also be brought to quiescence by giving the proper stimuli at the right time.

Note from Fig. 1 that there are the regions of bistability (i.e., the coexistence of the stable periodic and stable steady state branches). In these regions (i.e., from the left of PLP to HB and from the right of HB to PLP), the myocardium becomes very susceptible to impulses (since its action potential has two stable solutions at the same time). In the following, we study the phase resetting phenomenon in the bistability region of the right-hand side i.e., $I_{app} = 2.66 \mu A/cm^2$.

Fig. 4 shows phase resetting behavior of the myocardium in the presence of $I_{app} = 2.66 \mu A/cm^2$ when various magnitudes of hyperpolarizing current pulses were given at the same phase. Here, a perturbation pulse with a duration of 200 ms was delivered at -59 mV of the rising phase of the action potential. The times of application of current impulses are indicated by arrows. As shown in the top trace, a small current pulse of -0.1 $\mu A/cm^2$ perturbs and delays the subsequent oscillations. A stronger current pulse of -0.7 $\mu A/cm^2$ given at the same phase results in an instantaneous decrease in the oscillatory amplitude that leads to the steady state value, as shown by the second trace. A still stronger pulse of -1.3 $\mu A/cm^2$ merely advances the subsequent oscillations (see the third trace). Rhythmic activity in our simulation is restored from an inactive fiber by applying a perturbation current of sufficiently large magnitude (i.e., -2 $\mu A/cm^2$). (See the bottom trace, where the initial condition corresponds to the arrow of the second trace.) The trend shown in this figure agrees qualitatively with our earlier work on the Purkinje fiber (9).

In Fig. 5 we enlarged the unperturbed action potential in the previous figure to show a detail of its shape at a given spontaneous cycle. Here, the spontaneous cycle on the horizontal direction is defined as a fractional time into the unperturbed cycle, the origin of which is set at the absolute

minimum membrane potential. As indicated in this figure, the action potential can be roughly partitioned into four phases. Each phase is attributed to the following ionic events that take place on the surface of the membrane: The voltage-dependent Na^+ channel is almost inactive in the presence of $I_{app} = 2.66\ \mu A/cm^2$. Thus, an initial slow depolarization (phase 4) is mainly due to slow permeability of Ca^{2+} ions. The depolarization induced by Ca^{2+} entry enhances the Ca^{2+} conductance resulting in a faster depolarization (phase 0). This is followed by an initial phase of repolarization (phase 1), which is due to a slow inactivation of the Ca^{2+} channel and to the flow of an outward current carried by K^+ through the time-independent K^+ channel. The latter part of phase 1, which repolarizes faster than the initial repolarizing phase, is due to a gradual activation of the slow time-dependent K^+ channel. The ensuing phase 2 is characterized by a plateau repolarization; this is due to the near balance of the inward current I_s and the total outward current, $I_{k1} + I_{x1}$. The inactivation of the inward current and the progressive time-dependent activation of the slow outward current I_{x1} eventually lead to the termination of the plateau. A rapid repolarization (phase 3) starts when I_{x1} exceeds I_s.

Fig. 6 *a* shows phase resetting behavior of the fiber at different phases of the oscillatory cycle, obtained by scanning with a 200-ms current pulse of $-1.3\ \mu A/cm^2$. A brief hyperpolarizing pulse applied at the slowly depolarizing phase (i.e., the initial part of phase 4) merely results in advance in phase resetting, as shown in the top trace (in this case, the pulse was applied at -61 mV of the upstroke). On the other hand, if the pulse is applied during phase 0 (i.e., the fast depolarizing phase), there is a delay in the subsequent beat (see the second trace; here, the pulse is applied at -40 mV of the upstroke). The current pulse applied at phase 1 (i.e., the initial repolarizing phase) results in complete annihilation of the rhythmic activity (see the third trace; here, at 11 mV of the downstroke).

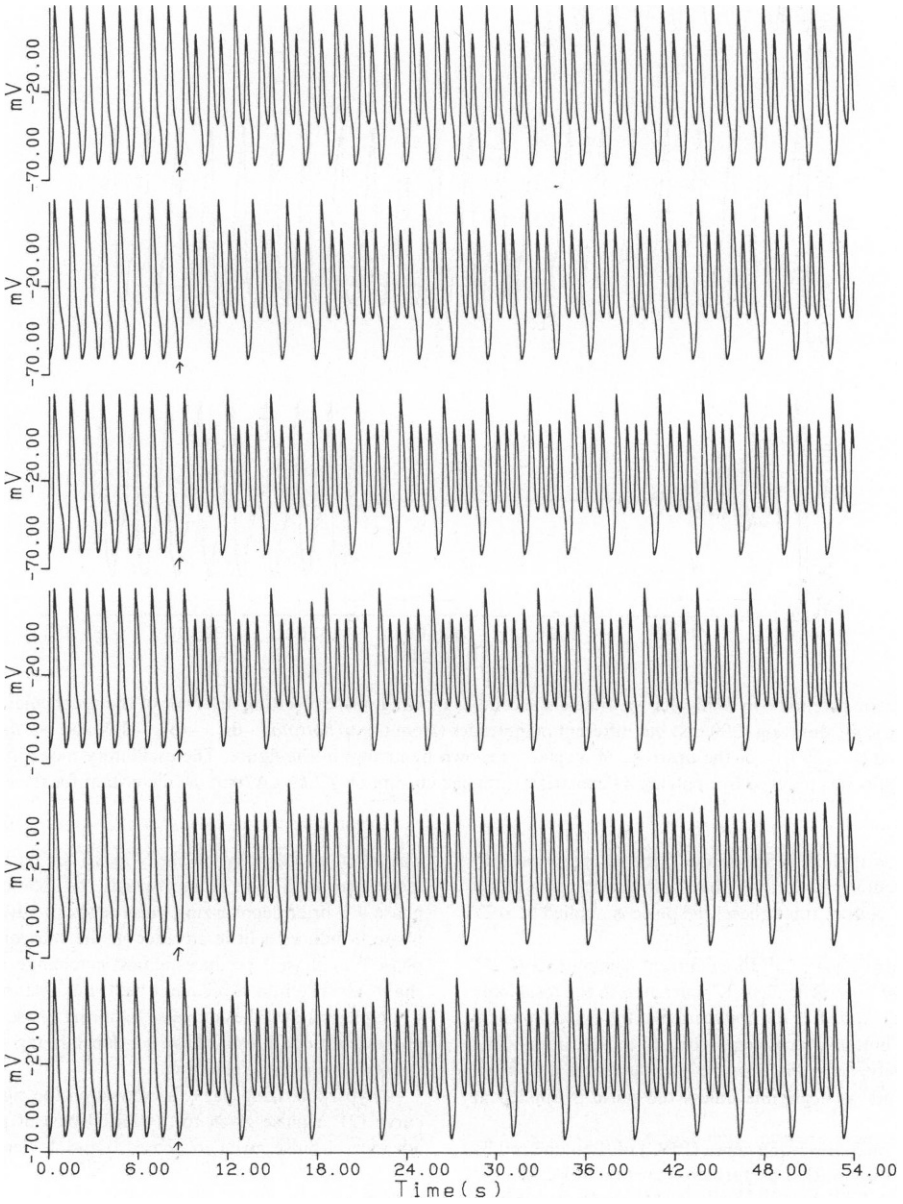

FIGURE 3 Spiking-bursting modes induced by instantaneously changing the strength of applied current at the arrows shown. Originally, the system was in a repetitive state at $2.6665\ \mu A/cm^2$; the strength of applied current is increased at the arrows shown (i.e., -61.04 mV of the upstroke) to 2.670, 2.6715, 2.6717, 2.6718, 2.67185, and $2.671855\ \mu A/cm^2$, running from the *top* trace to the *bottom*.

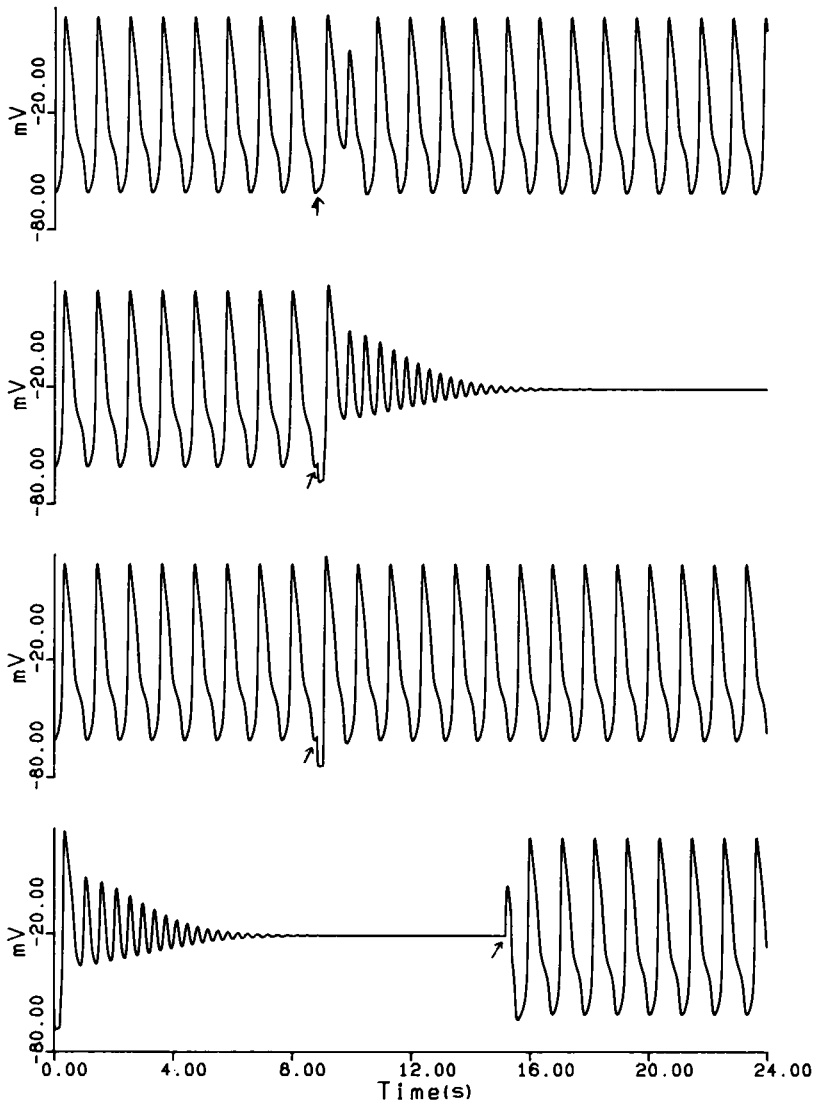

FIGURE 4 Membrane potential (in millivolts) vs. time (in seconds), showing phase resetting behavior of the ventricular muscle fiber, using current pulses of the same duration (200 ms) but different magnitudes (from *top* to *bottom*; -0.1, -0.7, -1.3, and $-2\ \mu A/cm^2$). Perturbing pulses were delivered at -59 mV of the upstroke of a spike as shown by arrows in the figure. The oscillatory mode in this figure and the subsequent four figures was induced by applying a depolarizing applied current of $+2.66\ \mu A/cm^2$, held constant for the entire duration.

When the same stimulus is applied during phase 2 (the plateau repolarizing phase), the fiber resumes its activity but with advance in phase resetting as shown in the bottom trace (here, the pulse is applied at -27 mV of the downstroke).

Fig. 6 *b* shows the contribution of all three current components (Ca^{2+} and time-independent and time-dependent K^+ currents) to the total ionic current just before, during, and after the application of the pulse shown on Fig. 6 *a*; here the top to bottom traces correspond to those traces of the previous figure, respectively. As in Fig. 2 *b*, the Na^+ current is not shown here because its magnitude is negligible unless the pulse is applied at phase 3 or phase 4.

Fig. 7 summarizes the phase resetting curve (PRC) of the same cell by scanning the pacemaker cycle with a perturbation current pulse of $+0.3$ $\mu A/cm^2$ (the left panel) and $-0.1\ \mu A/cm^2$ (the right panel), each with a duration of 200 ms. Here, we define the old phase as the unperturbed cycle and the new phase as the phase that appears in 6.540 ms (i.e., six times the basic cyclic length 1,090 ms) after applying the stimulus that was given at the point on the x axis (i.e., on the old phase).[2] A closer inspection of the left frame reveals the following observations: during phase 4 a brief depolarizing pulse tends to advance the phase resetting; phase 0 induces a little advance in the subsequent beat; a switch from phase 0 to phase 1 produces almost no change; during phase 1 there is a slight advance in a subsequent beat; the rhythmic fiber loses its activity when phase 1 switches to phase 2; during phase 2 there is a long delay in phase resetting; during phase 3 a depolarizing stimulus results in only a slight delay in phase resetting.

A hyperpolarizing pulse, as shown on the right panel, yields a type 0 curve (2): a pulse given to the initial part of phase 4 leads to a slight advance; a pulse given to phases 0 and 1 yields cessation in rhythmic

[2]We defined the new phase in this fashion because for some stimuli strengths, the ventricular myocardium starts to resume its normal cyclic activity after six complete basic cyclic lengths from the time of stimuli.

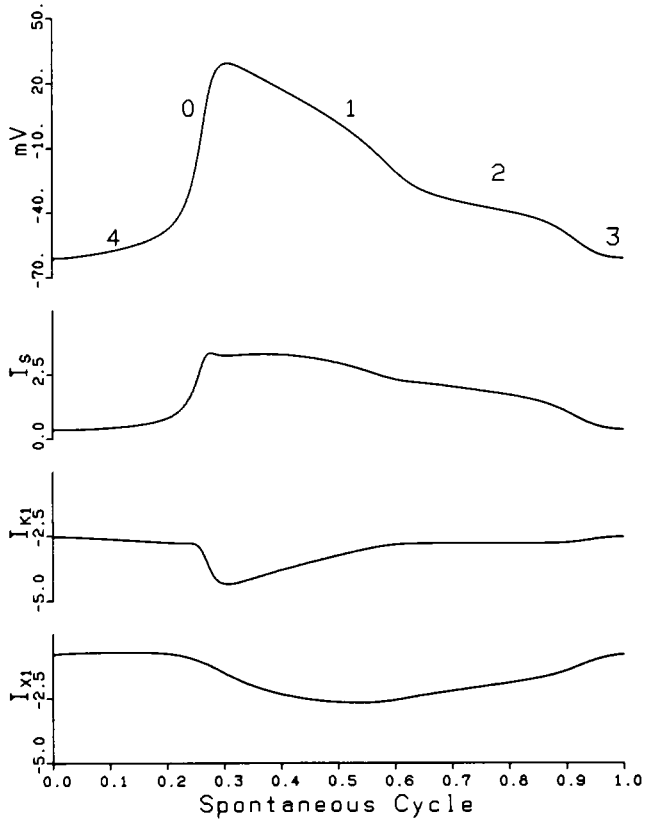

FIGURE 5 The action potential and its ionic composition in the presence of $I_{app} = 2.66\ \mu A/cm^2$. Here, I_s is an inward current carried mainly by Ca^{2+} ions through the slow time and voltage-dependent channel; I_{k1} is an outward current carried by to K^+ ions through the time-independent channel; and I_{x1} is another outward current carried by K^+ ions through the time-dependent channel. The spontaneous cycle is defined as a fractional time into the normal cycle such that the phase at the minimum potential is set at zero.

activity; and a pulse given to the later part of phase 1 and the entire part of phases 2 yield phase resetting but no cessation in rhythm; and finally a switch from phase 2 to phase 3 gives rise to a large downward jump resulting in delay in phase resetting.

In Fig. 8, we show phase resetting behavior as a current pulse of various magnitudes and of 200-ms duration scanned at intervals along the unperturbed cycle. The numbers in this figure are new phases expressed in the percent of the spontaneous cycle, and each line was obtained by connecting equal new phase values with the aid of the DISPLA software (14). The shaded areas are the regions (i.e., black holes) where the fiber ceases its rhythmic activity. Note that as in the Purkinje fiber (9), the ventricular myocardium is susceptible to both positive and negative stimuli. Note also that as in the Purkinje fiber, all the contour lines avoid to converge to these holes.[3]

DISCUSSION

Beeler and Reuter (12) have found that the rhythmic oscillatory potentials in the ventricular muscle fiber can be brought about by applying a steady depolarizing applied current. At a moderate depolarization, the fiber generated an oscillation cycle of about every 13 s. Our bifurcation analysis not only confirms their finding, but also shows that oscillatory potentials could be generated by a subthreshold applied current of $I_{sub} = 2.01\ \mu A/cm^2$ and terminated by a suprathreshold current of $I_{sup} = 2.68\ \mu A/cm^2$. The period of the stable oscillations is large near I_{sub} compared with that near I_{sup}. The amplitude varies only slightly for the entire range of the stable periodic solutions. Near I_{sup}, the oscillatory mode becomes a bursting type and sometimes chaotic, as shown in Fig. 3. In addition, the BR model predicts the existence of bistability in the ventricular muscle cell: a stable continuous oscillation and a time-independent stable steady state.

In the ventricular fiber, there are two Hopf bifurcation points whose neighborhood is susceptible to impulses. In these regions, brief current pulses can send the rhythmic fiber into quiescence, when it is applied at the proper phase and with the right magnitude. The stimuli vs. phase plot in Fig. 8 (which was obtained in the neighborhood of the right bifurcation) shows that the rhythmic activity of the ventricular myocardium is more susceptible to hyperpolarizing stimuli. Moreover, we find that the rhythmic ventricular cell near the left bifurcation point is much more susceptible to an impulse than that near the right bifurcation point. This can be seen in the top trace of Fig. 2, where only $0.005\ \mu A/cm^2$ was needed to annihilate the rhythm.

Our simulations indicate that intracellular calcium changes and the sodium current I_{Na} contribute very little to the phase responses. This can be seen from the bifurcation diagram shown in the top trace of Fig. 9, which was obtained using $E_s = 80$ mV (i.e., the variation in the intracellular calcium with time was set equal to zero). It is also evident in the bottom trace, which was constructed by setting ($E_s = 80$ mV and $g_{Nac} = 0$. Note that Fig. 9 retains the same qualitative features as Fig. 1 but is shifted toward the right, while maintaining the same qualitative features as Fig. 1. It is interesting to point out that bursting-spiking similar to those shown in Fig. 3 also exists in the vicinity of the right PLP in these reduced systems (i.e., the systems corresponding to the top trace and also that corresponding to the bottom trace).

Bursting and chaos shown in Fig. 3 seem to be a characteristic of all heart cells. In the Purkinje fiber, these phenomena have been observed for much wider ranges of I_{app}. Although the relevance of the bursting phenomenon to fibrillation is not obvious, it may provide an explanation for arrhythmia arising from a sick cell.

The PRC must be a useful tool for understanding the ionic current mechanisms that underlie phase resetting properties, as revealed from Fig. 6 *b*: Brief hyperpolarizing pulses introduced during a slow depolarization (phase 4) alter the interbeat interval as a result of the activation of I_{k1} and I_{x1}. The alteration in the interbeat during the fast depolarizing phase (phase 0) is attributed to an inactiva-

[3]This may be due to DISPLA software, which tends to connect all the points having equal phase shifts, in every possible way.

tion of the slow inward currents I_s and I_{k1}. Stimuli introduced during phase 1 reset the interbeat interval primarily by influencing the outward currents I_s and I_{x1}. Finally, brief pulses given at later times in the cycle affect the interbeat interval due to the alternation in all three currents.

The bifurcation analysis presented in Figs. 1 and 9 provides a convenient way of understanding how quiescent cardiac cells like the ventricular muscle cell can produce spontaneous rhythmic activity with an application of a steady depolarizing current. Apparently, this steady current can reduce the maximum diastolic potential (MDP) to a higher value (i.e., above the left HB). Although we have used I_{app} as a bifurcation parameter, in principle, any parameter in the model that affects MDP can be used as a bifurcation parameter. For example, automatic rhythm is known to arise from a quiescent fiber by varying external ionic concentrations such as Na^+ and Ca^{2+}, i.e., by altering the equilibrium potentials in the model. An increase in extracellular potassium concentration can reduce the MDP to the range where a quiescent cell can be converted to a pacemaker. Reduction of the activity of sodium and potassium pump of the cell as a result of some impairment of the metabolic activities could cause a reduced MDP. Indeed, there is strong evidence that, with ischemia, which leads to infarction, some fibers lose maximum diastolic potential and show automatic firing due to phase 4 depolarization (16). Also, some diseased human atrial tissues show phase 4 depolarization causing abnormal automatic firing (17). The cell having a reduced MDP is known to be sensitive to an impulse (16), and indeed this can be explained in terms of our bifurcation diagram (i.e., in terms of the existence of the bistability regions in our bifurcation diagram).

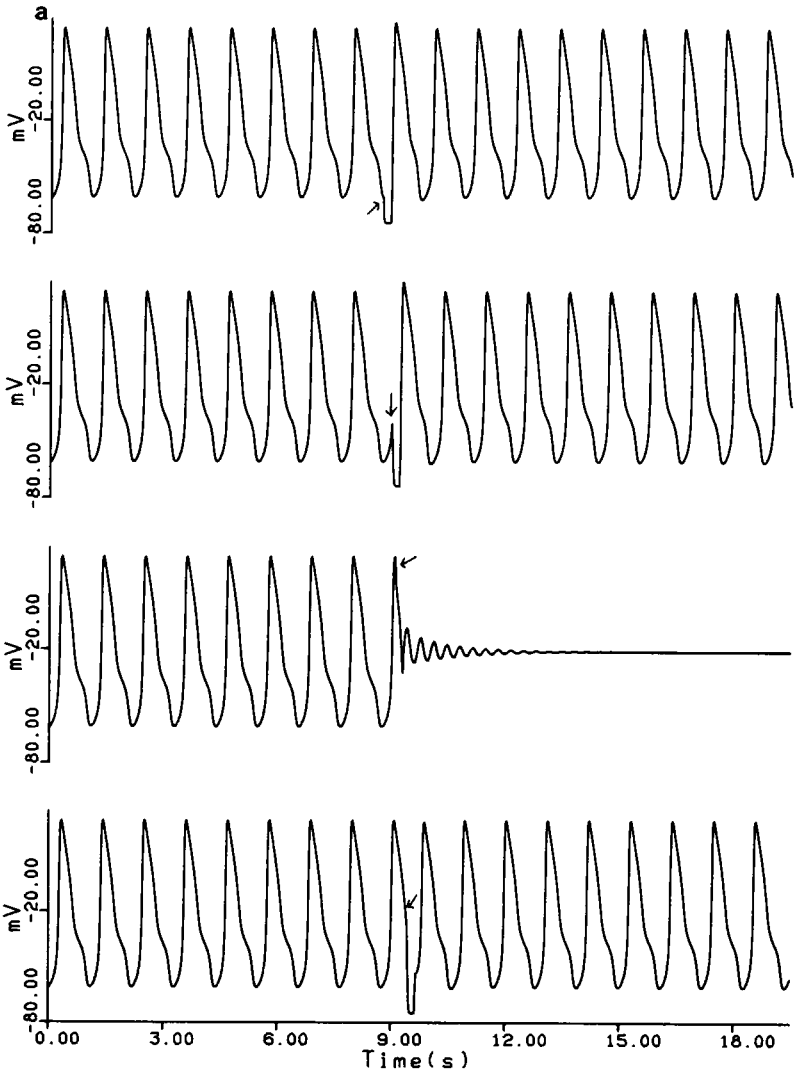

FIGURE 6 (*a*) Phase resetting behavior as in Fig. 4, but this time, a current pulse of $-1.3\ \mu A/cm^2$ was scanned at different phases (as shown by arrows) of the unperturbed cycle. From the *top* trace to *bottom*, the phases at which a brief pulse was applied are -61, -40 mV of the upstroke, $+11$ and -27 mV both during the downstroke. (*b*) The response of three currents to a brief pulse of *a* is shown.

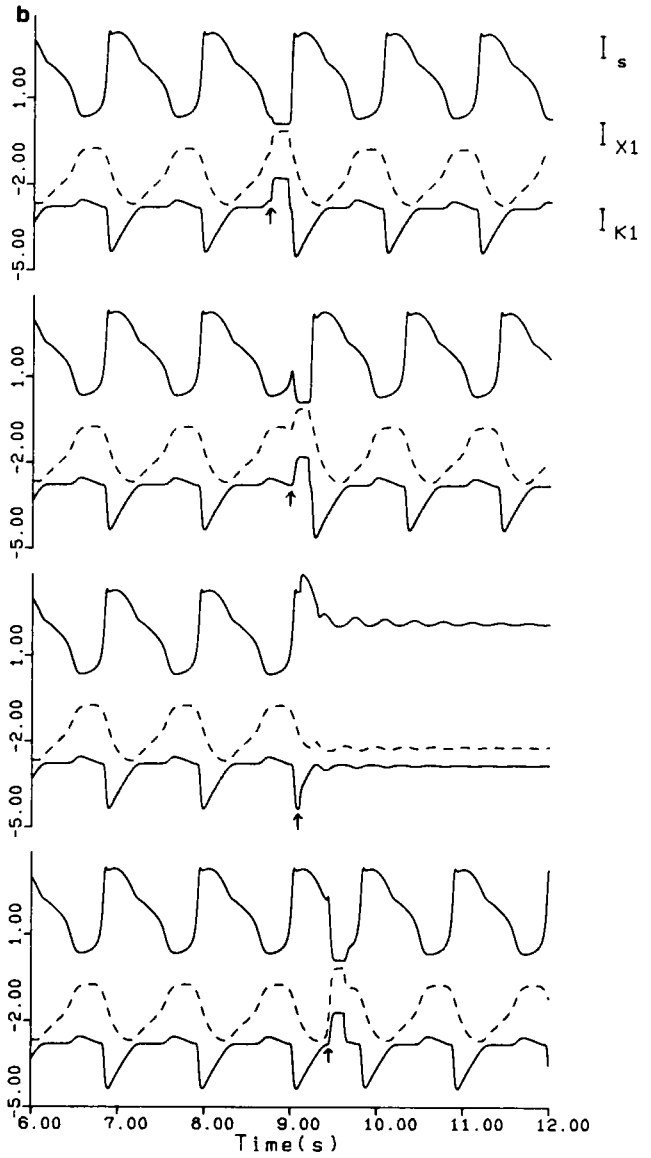

FIGURE 6 Continued

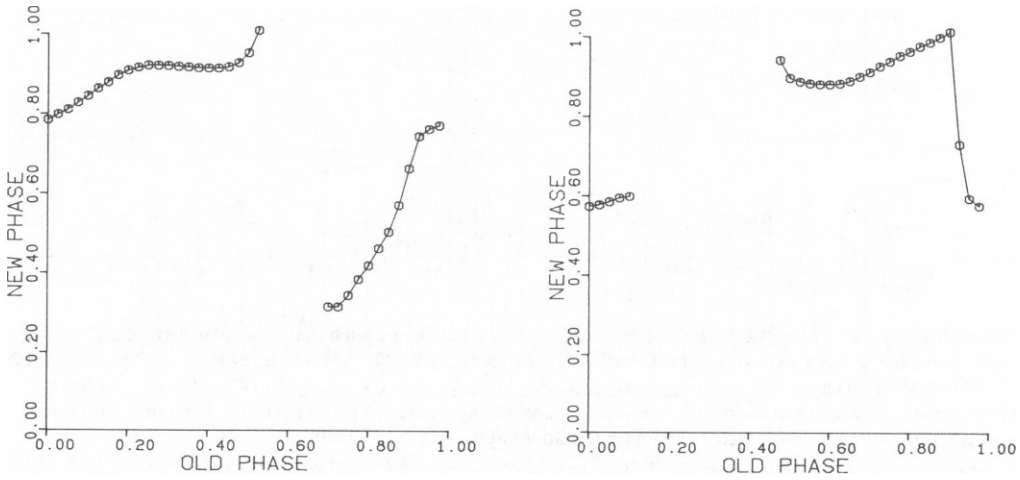

FIGURE 7 Phase resetting curve of the same cell using a current pulse of +0.3 (positive impulse, *left*) and −0.1 $\mu A/cm^2$ (negative impulse, *right*) and both for a duration of 200 ms by scanning different points in the pacemaker cycle.

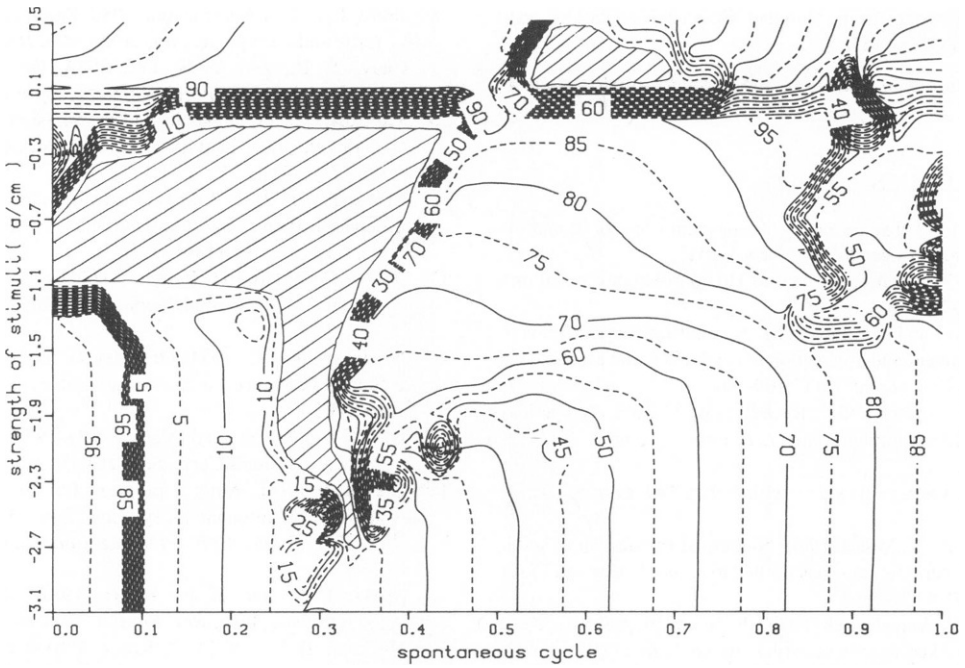

FIGURE 8 Stimuli vs. spontaneous cycle, obtained by giving both negative and positive brief current pulses. The numbers shown here refer to the new phases (in percent) that appeared 6,540 ms after given a brief stimulus (whose magnitude is given on the y-axis) at the point in the cycle on the x-axis. The contour lines were drawn by connecting equal new phase values with DISPLA software. The shaded areas are the regions where the fiber ceases its rhythmic activity.

Our simulations on the ventricular myocardium and Purkinje fiber indicate that given the appropriate conditions, the triggering of the initiation and termination of rhythmic activity must be a basic characteristic of all heart cells. We believe that the bifurcation analysis presented here is a fundamental way to learn the characteristics of the cardiac action potential and hope that our demonstration of the existence of black holes in the Purkinje fiber and ventricular myocardium may lead to a better understanding of the mechanism of normal as well as abnormal rhythms.

We would like to thank Professor Doedel at the Concordia University (Montreal, Canada) for providing us with his AUTO software tape. We would also like to thank Dr. John Rinzel at the National Institutes of Health and Professor Jame Franzen at the University of Pittsburgh (Pittsburgh, PA) for many helpful suggestions and illuminating discussions.

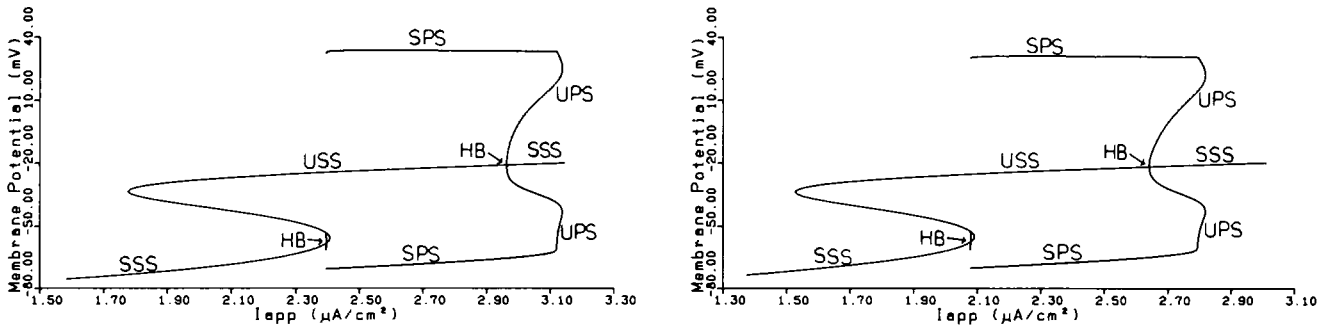

FIGURE 9 Bifurcation diagram of the BR equations where d[Ca]/dt was set at zero such that E_s = 80 mV (*top*) and that E_s = 80 mV and g_{Na} = g_{Nac} = 0 (*bottom*). In the *top* trace, two Hopf bifurcations appear at I_{app} = 2.080 μA/cm^2 (i.e., at V_m = −57.10 mV) and 2.641 μA/cm^2 (i.e., at V_m = −21.45 mV). Two knees (i.e., the limit points) appear at 1.526 μA/cm^2 (i.e., −33.58 mV) and 2.092 μA/cm^2 (i.e., −54.67 mV). The lower stable periodic limit point appears at 2.078 μA/cm^2 and the upper one at 2.796 μA/cm^2. The upper unstable periodic branch extends to 2.818 μA/cm^2. In the *bottom* trace, two Hopf bifurcations appear at I_{app} = 2.398 μA/cm^2 (i.e., at V_m = −57.75 mV) and 2.963 μA/cm^2 (i.e., at V_m = −20.85 mV). Two knees appear at 1.777 μA/cm^2 (i.e., −33.34 mV) and 2.407 μA/cm^2 (i.e., −55.50 mV). The lower stable periodic limit point appears at 2.395 μA/cm^2 and the upper one at 3.122 μA/cm^2. The lower unstable periodic branch starts from to 2.395 μA/cm^2 and the upper one extends to 3.138 μA/cm^2.

This work was supported by a National Science Foundation grant PCM79 22483 and PCM82 15583.

Received for publication 30 May 1984 and in final form 10 December 1984.

REFERENCES

1. Winfree, A.T. 1980. The geometry of biological time. *In* Biomathematics. Vol. 8. Springer-Verlag, New York.
2. Best, E. N. 1979. Null space in the Hodgkin-Huxley equations. *Biophys. J.* 27:87–103.
3. Hodgkin, A., and A. F. Huxley. 1952. A quantitative description of membrane current and application to conduction and excitation in nerve. *J. Physiol.* (*Lond.*). 117:500–544.
4. Guttman, R., S. Lewis, and J. Rinzel. 1980. Control of repetitive firing in squid axon membrane. *J. Physiol.* (*Lond.*). 305:377–395.
5. Rinzel, J. 1978. On repetitive activity in nerve. *Fed. Proc.* 37:2793–2802.
6. Rinzel, J., and R. N. Miller. 1980. Numerical calculation of stable and unstable periodic solutions to the Hodgkin-Huxley equations. *Math. Biosci.* 49:27–59.
7. Jalife, J., and C. Antzelevitch. 1979. Phase resetting and annihilation of pacemaker activity in cardiac tissue. *Science* (*Wash. DC*). 206:695–697.
8. Jalife, J., and C. Antzelevitch. 1980. Pacemaker annihilation: diagnostic and therapeutic implication. *Am. Heart J.* 100:128–130.
9. Chay, T. R., and Y. S. Lee. 1984. On impulse responses of automaticity in the Purkinje fibers. *Biophys. J.* 45:841–849.
10. McAllister, R. E., D. Noble, and R. W. Tsien. 1975. Reconstruction of the electrical activity of cardiac Purkinje fibers *J. Physiol.* (*Lond.*). 251:1–57.
11. Katzung, B. G. 1975. Effects of extracellular calcium and sodium on depolarization-induced automaticity in guinea pig papillary muscle. *Circ. Res.* 37:118–127.
12. Beeler, G. W., and H. Reuter. 1977. Reconstruction of the action potential of myocardial fibers. *J. Physiol.* (*Lond.*). 268:177–210.
13. Hindmarsh, A. C. 1974. Ordinary Differential Equation Systems Solver. Lawrence Livermore Laboratory, Livermore, CA. Report UCID-30001.
14. DISPLA User's Manual (Version 8.2). 1978. Section H. Integrated Software Systems Corp., San Diego, CA.
15. Doedel, E. 1981. Auto: a program for the automatic bifurcation analysis of autonomous systems. *Proc. Manitoba Conf. Num. Math. Comput., 10th, Winnipeg, Canada, Congr. Num.* 30:265–284.
16. Spear, J. F., and E. N. Moore. 1982. Mechanism of cardiac arrhythmias. *Annu. Rev. Physiol.* 44:485–497.
17. Hoffman, B. F., and M. R. Rosen. 1981. Cellular mechanisms for cardiac arrhythmias. *Circ. Res.* 49:1–15.